Inorganic Chemistry
Article
Cite This: Inorg. Chem. XXXX, XXX, XXX−XXX
pubs.acs.org/IC

Low-Spin Fe(III) Macrocyclic Complexes of Imidazole-Appended 1,4,7-Triazacyclononane as Paramagnetic Probes

Pavel B. Tsitovich,[†] Frédéric Gendron,[†] Alexander Y. Nazarenko,[‡] Brooke N. Livesay,[§] Alejandra P. Lopez,[†] Matthew P. Shores,[§] Jochen Autschbach,[†] and Janet R. Morrow*[,†]

[†]Department of Chemistry, University at Buffalo, State University of New York, Amherst, New York 14260, United States
[‡]Chemistry Department, State University of New York, College at Buffalo, 1300 Elmwood Avenue, Buffalo, New York 14222, United States
[§]Department of Chemistry, Colorado State University, Fort Collins, Colorado 80523, United States

Supporting Information

ABSTRACT: Two macrocyclic complexes of 1,4,7-triazacyclononane (TACN), one with *N*-methyl imidazole pendants, [Fe(**Mim**)]$^{3+}$, and one with unsubstituted NH imidazole pendants, [Fe(**Tim**)]$^{3+}$, were prepared with a view toward biomedical imaging applications. These low-spin Fe^{3+} complexes produce moderately paramagnetically shifted and relatively sharp ^{1}H NMR resonances for paraSHIFT and paraCEST applications. The [Fe(**Tim**)]$^{3+}$ complex undergoes pH-dependent changes in NMR spectra in solution that are consistent with the consecutive deprotonation of all three imidazole pendant groups at high pH values. *N*-Methylation of the imidazole pendants in [Fe(**Mim**)]$^{3+}$ produces a complex that dissociates more readily at high pH in comparison to [Fe(**Tim**)]$^{3+}$, which contains ionizable donor groups. Cyclic voltammetry studies show that the redox potential of [Fe(**Mim**)]$^{3+}$ is invariant with pH ($E_{1/2}$ = 328 ± 3 mV vs NHE) between pH 3.2 and 8.4, unlike the Fe(III) complex of **Tim** which shows a 590 mV change in redox potential over the pH range of 3.3−12.8. Magnetic susceptibility studies in solution give magnetic moments of 0.91−1.3 cm^3 K mol^{-1} (μ_{eff} value = 2.7−3.2) for both complexes. Solid-state measurements show that the susceptibility is consistent with a S = 1/2 state over the temperature range of 0 to 300 K, with no crossover to a high-spin state under these conditions. The crystal structure of [Fe(**Mim**)](OTf)$_3$ shows a six-coordinate all-nitrogen bound Fe(III) in a distorted octahedral environment. Relativistic *ab initio* wave function and density functional theory (DFT) calculations on [Fe(**Mim**)]$^{3+}$, some with spin orbit coupling, were used to predict the ground spin state. Relative energies of the doublet, quartet, and sextet spin states were consistent with the doublet S = 1/2 state being the lowest in energy and suggested that excited states with higher spin multiplicities are not thermally accessible. Calculations were consistent with the magnetic susceptibility determined in the solid state.

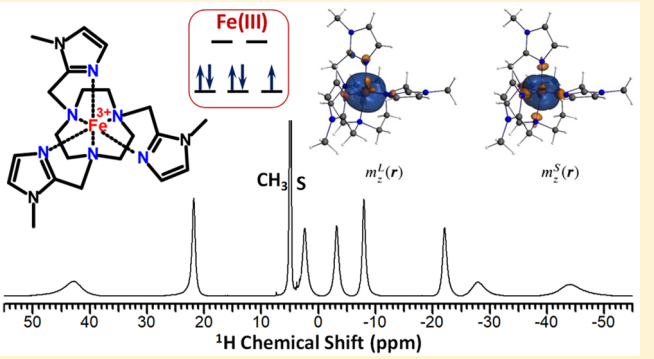

INTRODUCTION

There is renewed interest in the chemistry of paramagnetic macrocyclic complexes of Fe(II) and Fe(III) for biomedical imaging applications,[1−7] as well as for spin crossover materials for temperature-responsive imaging agents.[8,9] Paramagnetic iron coordination complexes are of interest as magnetic resonance imaging (MRI) contrast agents including T_1 agents[10,11] and paramagnetic chemical exchange saturation transfer (paraCEST) agents,[1,2,4−6] and as paraSHIFT agents for magnetic resonance spectroscopy (MRS).[3,12−14] Macrocyclic ligands are especially important in this regard since they form transition metal ion complexes which are robust toward dissociation of metal ion at neutral pH, 37 °C, and in the presence of competing ligands found in biological systems, such as carbonate, phosphate, and serum proteins.[15,16] Moreover, oxidation state and spin state must be controlled to produce a metal ion complex with magnetic properties that are favorable for these applications. Macrocyclic ligands facilitate the control of the inner coordination sphere of the metal ion center, especially if the metal ion is encapsulated by the macrocycle.

Recent research efforts have been dedicated to stabilization of high-spin divalent iron complexes for paraCEST imaging and paramagnetic shift ^{1}H NMR spectroscopy (paraSHIFT) applications.[1−3,5,6,13,14,16] These Fe(II) complexes have redox potentials as high as 0.8−1.0 V vs NHE[4,15] and encompass a variety of macrocyclic backbones including tetraaza- and triaza-macrocycles, as well as mixed oxa-aza macrocycles. Pendant groups attached to the macrocycle to encapsulate the Fe^{2+} ion

Received: April 14, 2018

DOI: 10.1021/acs.inorgchem.8b01022
Inorg. Chem. XXXX, XXX, XXX−XXX

for better control of coordination chemistry include amides and alcohols to form six,[1,2] seven,[16] or eight[6] coordinate complexes. Heterocyclic pendants have also been studied, including derivatives of pyridine groups that stabilize divalent Fe(II) complexes.[1−3] Notably, 1,4,7-triazacyclononane (TACN) appended with three heterocyclic donors that contain five-membered rings, such as benzimidazole, imidazole, or pyrazole, produce a coordination sphere which stabilizes Fe(III) relative to Fe(II).[17,18] The stabilization of Fe(III) by all-nitrogen donors is not common. More typically, anionic oxygen pendants such as depronated phenol,[19−22] alcohol,[23] or carboxylate[24,25] pendants form stabilized Fe(III) complexes as shown by more negative redox potentials for the Fe^{3+}/Fe^{2+} redox couples. A rare example of an Fe(III) complex with all-nitrogen donor pendants contains TACN with three deprotonated aminobenzyl pendants.[26]

Most Fe(III) complexes of macrocycles based on TACN are in the high-spin $S = 5/2$ state, including those that have oxygen pendants[19,22] and nitrogen pendants that form six-membered rings.[26] However, the small cavity size of TACN and strong ligand donor environment may promote the formation of low-spin Fe(III). Studies showed that an Fe(III) bis-TACN complex was low-spin.[27] Recent studies of iron complexes of TACN containing two pyridine pendant groups show a low-spin $S = 1/2$ Fe(III) center.[28]

In our efforts to explore the different coordination environments for Fe(II) and Fe(III) MRI contrast agents and paraSHIFT agents, we discovered rare examples of highly water-soluble and kinetically inert complexes of Fe(III) that contain all-nitrogen donors.[29] These complexes provide examples of low-spin Fe(III) as shown by NMR data and magnetic susceptibility studies, both in solution and solid state. The Fe(III) complex of **Tim** is ionizable over a wide pH range, producing species with several different protonation states. This complex demonstrated pH-dependent redox potential, while being extremely stable under both acidic and basic conditions over prolonged times. These complexes are proposed for application as electrolytes in redox-flow battery (RFB) applications.[29] Here we report further studies on the electrochemistry, NMR spectroscopy, and magnetic measurements of these complexes. These studies are supported by theoretical calculations that predict the predominance of the $S = 1/2$ state in these complexes. Such low-spin robust Fe(III) complexes produce relatively sharp proton resonances that suggest this new class of complexes will be useful for development as paraCEST or paraSHIFT agents, which require hyperfine-shifted exchangeable or nonexchangeable proton resonances, respectively.

RESULTS AND DISCUSSION

Fe(III) complexes of two different macrocycles with appended imidazole groups, abbreviated as **Mim** and **Tim**, were synthesized (Scheme 1). These two complexes were compared with the goal of understanding the effects of the imine donor groups on stability, spin state, paramagnetic-induced ^{1}H NMR shifts, and redox properties of the Fe(III) center. In the case of **Mim**, the imidazole nitrogen is capped with a methyl group, while **Tim** contains unsubstituted NH sites. This difference gives ionizable protons on the pendants of **Tim** (Scheme 2), whereas $[Fe(\mathbf{Mim})]^{3+}$ does not have pendant groups which ionize. Deprotonation of the NH groups of the imidazole heterocycles is of interest to stabilize the Fe(III) center through formation of anionic donor groups. In this regard,

Scheme 1

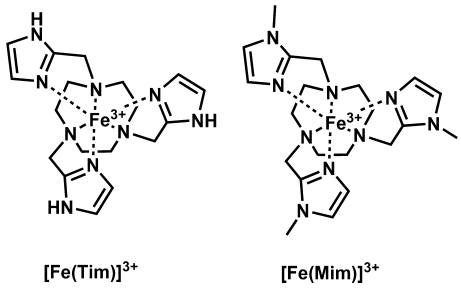

Fe(II) and Fe(III) complexes of tripodal chelates with pendant imidazoles have been reported.[30,31] Fe(II) imidazole pK_a values range from 8.5 to 9.5 for the tripodal ligands, whereas the large Lewis acidity of Fe^{3+} ion lowers the pK_a values of the tripodal ligands to 7.0, 7.5, and 8.8 in the methanol−water mixtures.[30]

Synthesis and Structure. Acid-catalyzed reductive amination in the presence of sodium triacetoxyborohydride was employed for the preparation of heterocycle-appended macrocyclic ligands.[32,33] The preparation of the **Tim** ligand from TACN and imidazole-2-carboxaldehyde required prolonged reaction times (8−10 days), while affording the final product in good yield.[29] The **Mim** ligand was synthesized from 1-methylimidazole-2-carboxaldehyde in excellent yield using a similar procedure with a shorter reaction time of 2 days (Scheme S1). Utilization of the acid-catalyzed reductive amination allowed for higher yields of the final products compared to traditional alkylation with aryl halides under basic conditions. Notably, the alkylation of TACN with acyl halides under basic conditions often results in mixtures of di- and trisubstituted products. Thus, the acid-catalyzed reductive amination has significant advantage over alkylation at basic conditions,[33] giving higher overall yield of trisubstituted product. $[Fe(\mathbf{Tim})]^{3+}$ and $[Fe(\mathbf{Mim})]^{3+}$ complexes were synthesized from iron(III) trifluoromethanesulfonate and purified using a modification of a procedure that has been recently developed.[29]

The complex cation of $[Fe(\mathbf{Mim})](CF_3SO_3)_3$ has a distorted octahedral geometry (Figure 1), with average bite angles of 83.1(2)° (Table S4) and with twist angles of 47(1)° (Figure S23). The coordination polyhedron deviates from the octahedron bite angle of 90° and twist angle of 60°. Planes of the lower triangle consisting of the TACN nitrogens and the upper triangle are nearly parallel with the angle between them of 1.2(1)°. The Fe−N average distances are 2.00(1) Å for aliphatic nitrogen atoms and 1.93(1) Å for imidazole nitrogen atoms (Table S4). These values are similar to those reported for the low-spin tris(1,10-phenathroline) Fe(III) complex (1.97 Å).[34] However, these bond lengths are much shorter than the ones reported for the Ni(II) complex of **Mim**.[35] The Fe−N bond distances and angles are similar to those reported for $[Fe(\mathbf{Tim})](OTf)_3$.[29] Metal ion complexes of TACN with three pendant groups have two elements of chirality associated with the conformation of the macrocycle backbone ($\delta\delta\delta$ or $\lambda\lambda\lambda$) and the direction of the swirl of the pendent groups.[3,12] In these complexes, the conformation of the backbone of the TACN ring is the same for all ethylene units: $(G^+C^+A^-)_3$ or [333] in Boeyens notation. In the Fe(III) complex studied here, the pendent groups and macrocyclic backbone correspond to the $\Lambda(\lambda\lambda\lambda)$ stereoisomer. Overall, the complex

DOI: 10.1021/acs.inorgchem.8b01022
Inorg. Chem. XXXX, XXX, XXX−XXX

Scheme 2. pH-Dependent Speciation of the [Fe(Tim)]$^{3+}$ Complex

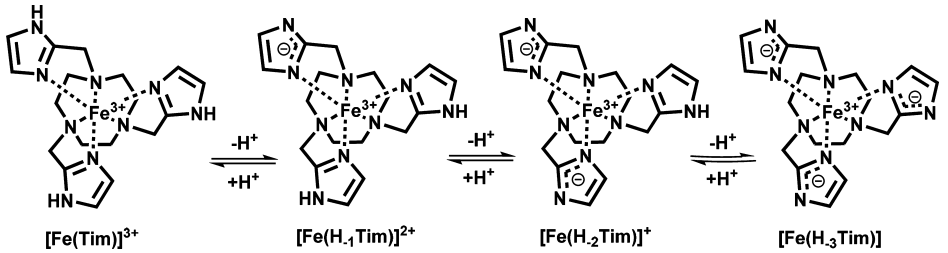

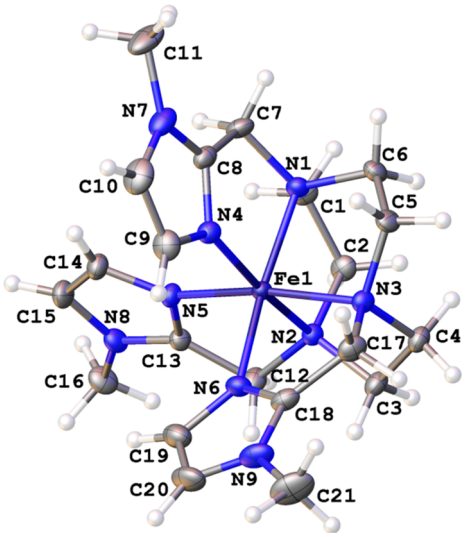

Figure 1. ORTEP molecular structure of the [Fe(**Mim**)]$^{3+}$ cation, showing the atom-labeling scheme and 50% probability displacement ellipsoids.

cations and triflate anions form an ionic crystal with no usual hydrogen bonds but with numerous C−H···O and C−H···F short contacts that may stabilize the crystal structure (Figure S22).

NMR Spectroscopy. The solution ^{1}H NMR spectra of both complexes are consistent with low-spin Fe(III) complexes (Figure 2). The ^{1}H resonances are relatively sharp and moderately paramagnetically shifted as typical of low-spin Fe(III) (Figures 2), whereas high-spin Fe(III) typically shows broader ^{1}H resonances.[36] For [Fe(**Mim**)]$^{3+}$, there are eight proton resonances of equal intensity and one resonance of 3-fold higher intensity, while [Fe(**Tim**)]$^{3+}$ demonstrates a similar ^{1}H NMR spectrum with eight proton resonances. The paramagnetically shifted proton resonances span from −45 to +45 ppm, while two resonances of [Fe(**Mim**)]$^{3+}$ and one of [Fe(**Tim**)]$^{3+}$ are found within the diamagnetic region. The proton resonance of [Fe(**Mim**)]$^{3+}$ at 5 ppm that has a 3-fold higher integration intensity is assigned to the *N*-methyl groups.

The ^{1}H NMR spectra of [Fe(**Mim**)]$^{3+}$ and [Fe(**Tim**)]$^{3+}$ are consistent with a single diastereomer predominating in solution. That the ^{1}H NMR spectra of the two complexes resemble each other under these conditions suggests the two complexes have similar geometries in solution. The major difference in the solution chemistry of the complexes is the presence of ionizable NH groups on the imidazole pendants of [Fe(**Tim**)]$^{3+}$, but not [Fe(**Mim**)]$^{3+}$. In fact, [Fe(**Tim**)]$^{3+}$ complex has been shown to deprotonate at all three imidazole-pendants, with pK_a values of 6.8 ± 0.1, 8.4 ± 0.2, and 9.8 ± 0.2 as determined by pH-potentiometric titrations (Scheme 2).[29] At high pH (>11), there is an additional ionization which is assigned to the formation of [Fe(**H**$_{-3}$**Tim**)(OH)]$^-$. In this complex, the hydroxyl group is most likely hydrogen bound in an outersphere interaction with the imidazole pendants, although we cannot exclude an inner-sphere interaction.[29,37] The pD dependence of the proton NMR spectrum of the Fe(III) complex of **Tim** reflects these ionization events, if the expected difference of approximately 0.5 pH unit of ionization events in D_2O is taken into account (Figure S1). Under acidic conditions where [Fe(**Tim**)]$^{3+}$ is the predominant species present, the proton NMR spectrum shows the simple eight resonances that are characteristic of a rigid complex of high symmetry. As the first pK_a is approached at pD 6.4, the proton resonances are substantially broadened and slightly shifted toward the diamagnetic region. With further increase of pD to 7.6, which is more alkaline than the first ionization, the proton resonances coalesce, and most of the resonances disappear into the baseline with only a few remaining. In the pD range of 8.6−11.5 there are multiple species in solution that differ by protonation state. The proton resonances become sharper at pD ≥ 11.5, suggesting that another dominant protonation state is present. At pD > 12.7, the predominant species is both [Fe(**H**$_{-3}$**Tim**)] and [Fe(**H**$_{-3}$**Tim**)(OH)]$^-$. The proton resonances are less shifted at pD 12.7 compared to those at pD ≤ 4.7, yet the paramagnetic shifts are observed for the entire pD range from pD 1.9 to 12.7. These data confirm the deprotonation of the imidazole groups as measured previously by pH-potentiometric titrations and by UV−vis spectroscopy (Figure 3). This pronounced pH dependence of the hyperfine shifted proton resonances highlights the potential of this complex for development as paraSHIFT agents based on Fe(III).[12,13]

The temperature dependence of the ^{1}H NMR resonances of the two complexes was studied to determine their suitability as paraSHIFT agents. Shown in Figures S2 and S3 are the ^{1}H NMR spectra of the [Fe(**Tim**)]$^{3+}$ complex at two different temperatures, including 25 and 55 °C at both pH 4.7 and 6.4. As anticipated for paramagnetic complexes, the proton resonances shift toward the origin as the temperature is increased.[3] However, a few of the resonances broaden and merge together at the higher temperature, suggesting that there is a dynamic process in solution. Apparent coalescence of certain resonances occurs in the spectra of this complex both at pH 4.7 and 6.4. At pH 6.4, all resonances are broadened due to the presence of multiple ionization states. The lack of sharp highly shifted proton resonances at higher temperatures suggests that [Fe(**Tim**)]$^{3+}$ will not be useful for application as a temperature dependent paraSHIFT probe.

The ^{1}H NMR spectra of [Fe(**Mim**)]$^{3+}$ at two temperatures are shown in Figure S4. The *N*-methyl resonances of the pendents of this complex would normally be chosen for paraSHIFT applications due to their larger integrated intensity

DOI: 10.1021/acs.inorgchem.8b01022
Inorg. Chem. XXXX, XXX, XXX−XXX

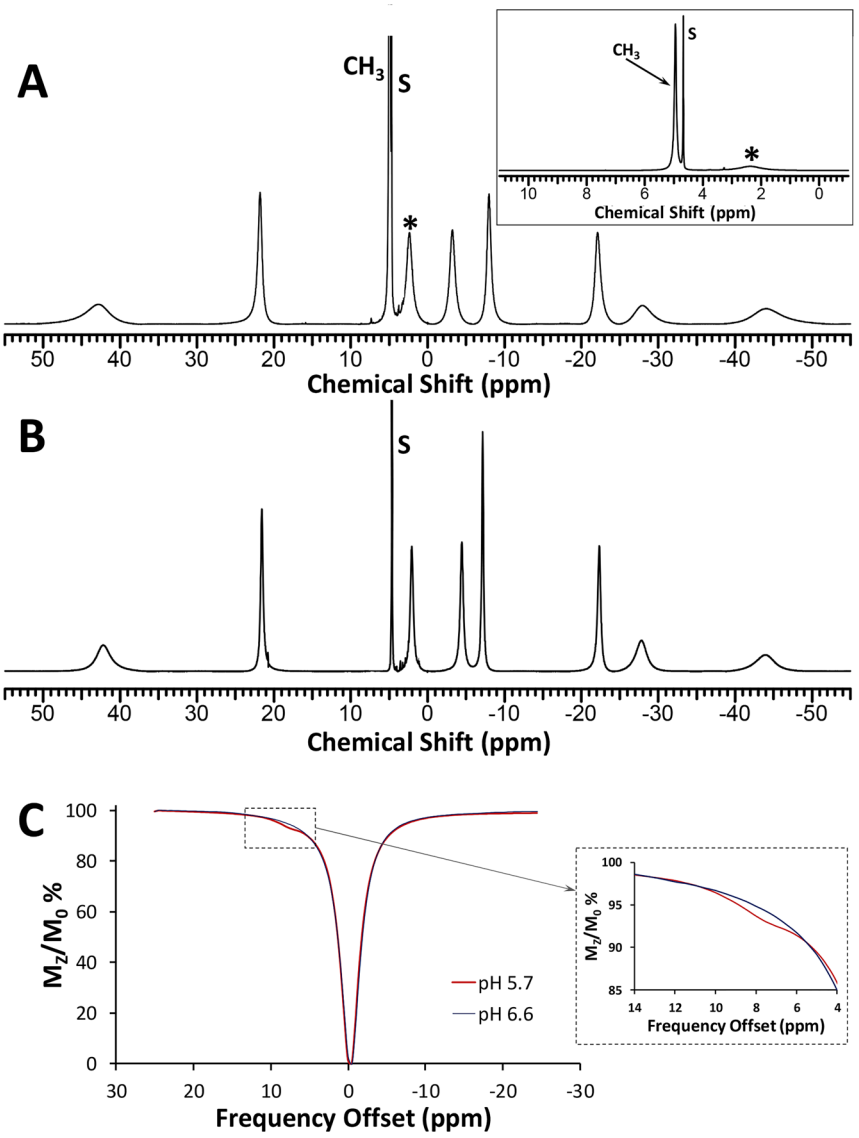

Figure 2. ^{1}H NMR spectra of (A) [Fe(**Mim**)]$^{3+}$ in D_2O at pD 6.5 with inset showing expanded diamagnetic region and (B) [Fe(**Tim**)]$^{3+}$ in D_2O at pD 4.8, 25 °C. *, intensity of this proton resonance of [Fe(**Mim**)]$^{3+}$ demonstrates the difference in scales. The solvent peak is labeled "S". (C) CEST effect of 25 mM Fe(**Tim**) observed at pH 5.7, 25 °C. Conditions: 40 mM MES, 100 mM NaCl in H_2O.

compared to other protons in the complex. However, in this case, the proton resonances are found at approximately 5 ppm and are thus not sufficiently highly shifted from bulk water for an optimal paraSHIFT agent.[38] Instead, the proton at −45 ppm is monitored as a function of temperature to give a temperature coefficient (CT) of 0.45 ppm °C^{-1} as shown in Figure S4. This value shows that the low-spin Fe(III) center may produce substantial CT values that are similar to those observed for divalent transition metal complexes.[3,14]

CEST NMR Spectroscopy. The [Fe(**Tim**)]$^{3+}$ complex was studied as a paramagnetic chemical exchange saturation transfer (paraCEST) agent. In initial studies, the exchangeable imidazole NH proton resonance was located at approximately 12 ppm in deuterated acetonitrile (Figure S5). CEST spectra, which show the percent water magnetization as a function of presaturation pulse frequency, are shown in Figure 2. There is a weak CEST peak at approximately 8 ppm versus bulk water at pH 5.7 and 25 °C which is in a similar location to that identified in the proton NMR in acetonitrile. This CEST peak appears as a shoulder at the higher temperature of 37 °C at pH 5.7 (Figure S6). However, the CEST effect disappears at pH 6.6, 25 °C (Figure 2). This disappearance is attributed to an increase in the proton exchange due to base catalyzed exchange. At near neutral pH, the rate of exchange is likely too fast to produce a CEST peak given that the resonance is not highly shifted from that of bulk water.[4,39] To further characterize the [Fe(**Tim**)]$^{3+}$ complex, the T_1 water proton relaxivity at pH 7.0 was measured at 4.7 T over the concentration range of 0.50−8.0 mM complex. The relatively low value of 0.06 mM^{-1} s^{-1} that was obtained is well within the range observed for divalent transition metal ion paraCEST agents under similar conditions and field strength. This result suggests that the lack of an strong CEST effect is not attributable to a large T_1 relaxivity.[5]

UV−Vis Spectroscopy. Electronic absorption spectroscopy was used to probe the solution speciation of the complexes as a function of pH. Both Fe(III) complexes of **Mim** and **Tim** show UV−vis absorbance peaks attributed to ligand electronic transitions (Figure 3). The Fe(III) complex of **Tim** is stable from pH 2.7 to 12.0 and shows isosbestic points over the pH

DOI: 10.1021/acs.inorgchem.8b01022
Inorg. Chem. XXXX, XXX, XXX−XXX

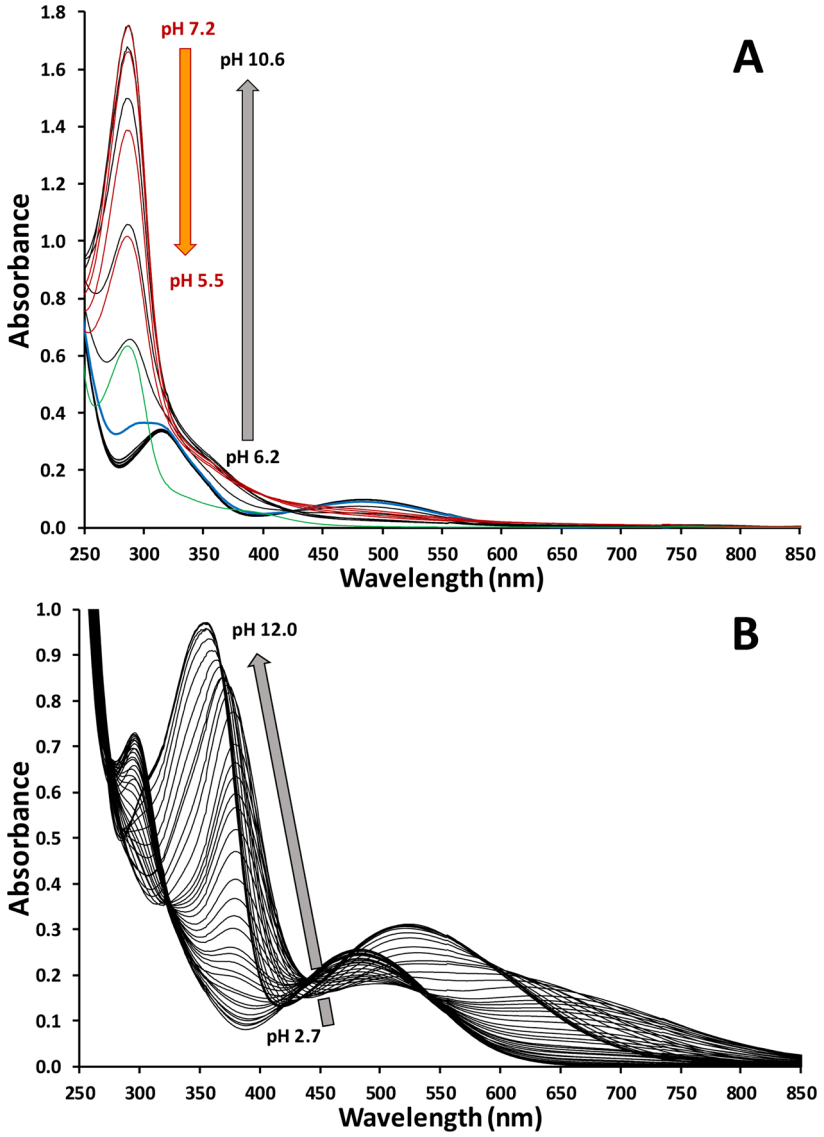

Figure 3. pH-dependence of the UV−vis spectra of (A) 0.86 mM Fe(**Mim**) at pH ≤ 10.6, where green line represents pure **Mim** (black lines, titration from pH 6.2 to pH 10.6; red lines, titration from pH 10.6 to pH 5.5); (B) 0.34 mM **Fe(Tim)** at pH 2.7−12.0. Conditions: 20 mM MES, 100 mM NaCl in H_2O at 37 °C. pK_{a1} 6.7, pK_{a2} 8.4, and pK_{a3} 9.7 are obtained from the fit.

2.7−7.6 titration range with a further shift in peak wavelength at pH > 7.6 that tracks the species present in solution as the imidazole pendants completely ionize at strongly alkaline conditions.[29] The pK_a values determined from the fit of the UV−vis data are 6.7, 8.4, and 9.7 (Figure S8), which matches the pH-potentiometric titration results. The complex is remarkably stable over this large pH range, in part because the anionic imidazole pendants stabilize the Fe(III) complex at basic pH. In contrast, the $[Fe(\mathbf{Mim})]^{3+}$ complex is stable only over a narrower pH range. As the pH of the solution is increased above pH 9.2, the metal-to-ligand (MLCT) charge-transfer band at λ = 484 nm disappears, while the $\pi-\pi^*$ absorbance band at λ = 287 nm for free ligand increases in intensity, suggesting that alkaline conditions promote dissociation of $[Fe(\mathbf{Mim})]^{3+}$ (Figures 3 and S7). Moreover, UV−vis spectral changes observed at pH ≥ 9.2 are only partially reversible as the pH is brought back to acidic values. These UV−vis data together with the observation of a precipitate at alkaline conditions suggest that the $[Fe(\mathbf{Mim})]^{3+}$ complex partially dissociates at basic pH with the formation of a free ligand and iron hydroxide precipitate.

Electrochemistry. Solution speciation and stability toward dissociation was also monitored through electrochemical studies. The cyclic voltammogram for $[Fe(\mathbf{Mim})]^{3+}$, shown in Figure 4, demonstrates a quasi-reversible wave with an $E_{1/2}$ of 328 ± 3 mV versus NHE at pH 5.6 with a slight linear effect of the scan rate variation on the peak separation. Notably, the redox potential does not change substantially over the pH range of 3.2−9.6 (Figures S9−S12). However, under basic conditions of pH 9.6, additional waves appear, consistent with dissociation of the complex. Return of the pH to neutral shows that the new waves characteristic of the impurities remain (Figure S12). Comparison of these experiments to the UV−vis spectra at high pH suggests that $[Fe(\mathbf{Mim})]^{3+}$ complex decomposes at high pH. $[Fe(\mathbf{Tim})]^{3+}$ complex, as reported previously,[29] shows a reversible wave at $E_{1/2}$ = 315 ± 6 mV vs NHE in water, which is constant at acidic pH ≤ 6.5, conditions under which the complex is fully protonated. Higher pH values produce deprotonation at the imidazole pendants and shift the

DOI: 10.1021/acs.inorgchem.8b01022
Inorg. Chem. XXXX, XXX, XXX−XXX

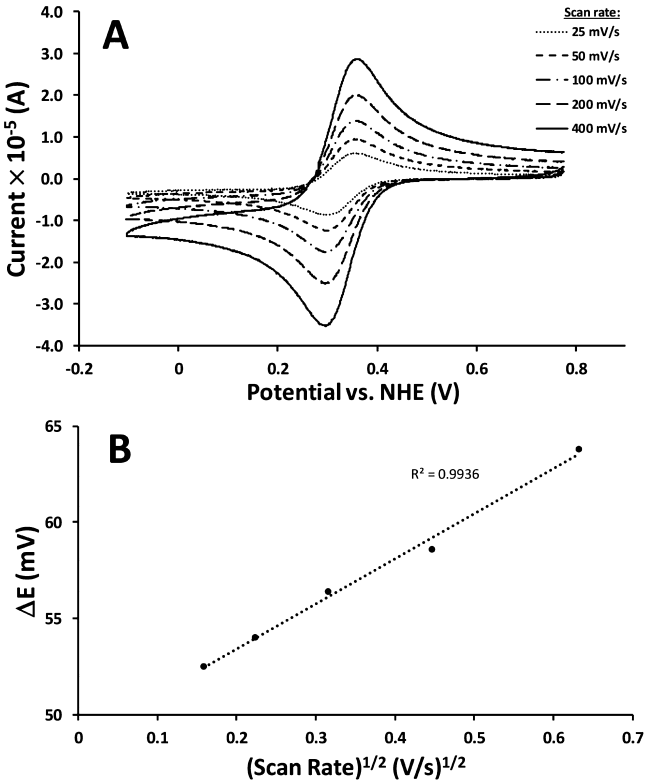

Figure 4. (A) Cyclic voltammograms of 1.8 mM $[Fe(\mathbf{Mim})]^{3+}$ at pH 5.6 in 1 M KCl solution (25 °C) at various scan rates, $E_{1/2}(Fe^{3+}/Fe^{2+})$ = 328 ± 3 mV vs NHE. (B) Quasi-reversible ΔE variation with the scan rate for the Fe^{3+}/Fe^{2+} redox couple of $[Fe(\mathbf{Mim})]^{3+}$ recorded at a glassy carbon working electrode at pH 5.6.

redox potential to negative values of $E_{1/2}$ = −270 ± 5 mV at pH 12.8 vs NHE, consistent with stabilization of $[Fe(\mathbf{H_{-3}Tim})]$ species at high pH. Notably, $[Fe(\mathbf{Mim})]^{3+}$ is stable toward dissociation at pH 3.6 to 8.4 over several hours, but not at higher pH values of 9.6. In contrast, $[Fe(\mathbf{Tim})]^{3+}$ showed no evidence of dissociation at high pH (pH 12) or low pH (pH 3.3) over a period of hours as observed by cyclic voltammetry or by UV−vis spectroscopy, even upon cycling back and forth between acidic and basic pH.[29]

Magnetic Properties of the Complexes in Solution and Solid State. To characterize the oxidation and spin states of $[Fe(\mathbf{Tim})]^{3+}$ and $[Fe(\mathbf{Mim})]^{3+}$ complexes in solution, the magnetic moments of these complexes were measured using the Evans method[40] as compiled in Table S5. The $[Fe(\mathbf{Tim})]^{3+}$ complex has a $\chi_M T$ value of 0.98 ± 0.0 cm^3 K mol^{-1} (μ_{eff} value = 2.8 ± 0.1) at neutral conditions in D_2O at 25 °C. A similar value of 1.1 ± 0.0 cm^3 K mol^{-1} (μ_{eff} value = 3.0 ± 0.1) was found for $[Fe(\mathbf{Mim})]^{3+}$. The pH and temperature effects on the magnetic moments of the Fe(III) complex of **Tim** were further studied. Only a slight change from 0.91 ± 0.0 to 1.3 ± 0.0 cm^3 K mol^{-1} (μ_{eff} value = 2.7 ± 0.0 to 3.2 ± 0.0) at 25 and 55°, respectively, was obtained at pD 8.5. Moreover, while there is no obvious pH effect on the values of magnetic moment, there is a slight increase observed at the elevated temperature under alkaline conditions. These values at 25 and 55 °C are higher than expected for an S = 1/2 state based on a spin-only contribution moment ($\chi_M T$ = 0.37 cm^3 K mol^{-1}, μ_{eff} value = 1.7).[41] A substantial spin−orbit coupling contribution that increases this value was confirmed by the theoretical calculations discussed below.

To further understand magnetic properties of these complexes and noting the increased interest in spin-crossover Fe(III) complexes,[42−44] we investigated the magnetic properties of the complexes over a broad temperature range. The temperature dependence of the magnetic susceptibility for solid-state samples of $[Fe(\mathbf{Tim})](OTf)_3$ and $[Fe(\mathbf{Mim})](OTf)_3$ are presented in Figure 5. At 300 K, the $\chi_M T$ values are

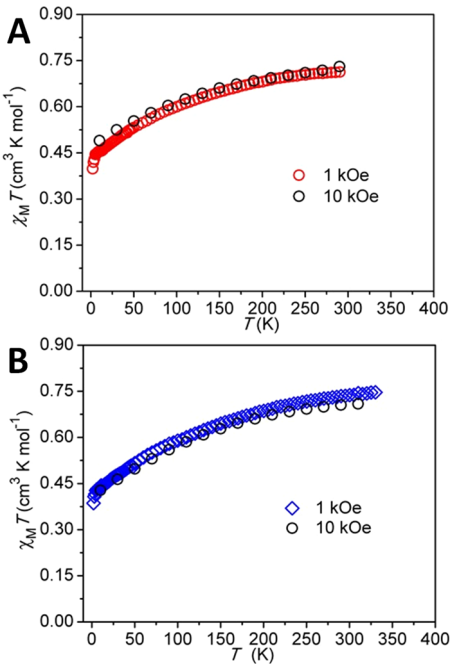

Figure 5. Temperature dependence of magnetic susceptibility for solid samples of (A) $[Fe(\mathbf{Tim})](OTf)_3$ and (B) $[Fe(\mathbf{Mim})](OTf)_3$ collected at applied fields of 1000 and 10 000 Oe.

0.70 cm^3 K mol^{-1} (μ_{eff} value = 2.3) and 0.74 cm^3 K mol^{-1} (μ_{eff} value = 2.4), respectively, higher than what is expected for a low-spin Fe(III) for a spin-only contribution (0.38 cm^3 K mol^{-1} when g = 2.0, μ_{eff} value = 1.7).[28,41] A similar room temperature $\chi_M T$ value of 0.68 cm^3 K mol^{-1} (μ_{eff} = 2.3) has been observed for a low-spin Fe(III) complex with a 1*H*-pyrazol-3-methylene appended-TACN ligand,[18] and it is likely that unquenched orbital angular momenta contribute to these higher-than-expected susceptibility values. Upon decreasing the temperature, the $\chi_M T$ values decrease gradually until ∼10 K, where the decrease becomes more pronounced until 2 K where the $\chi_M T$ values are 0.40 cm^3 K mol^{-1} (μ_{eff} value = 1.8) and 0.39 cm^3 K mol^{-1} (μ_{eff} value = 1.8) for $[Fe(\mathbf{H_3Tim})](OTf)_3$ and $[Fe(\mathbf{Mim})](OTf)_3$, respectively. Assuming S = 1/2 ground states, based on saturation magnetization measurements showing one unpaired electron per formula unit (Figures S14−S19), the downturns in magnetic susceptibilities at low temperature are likely due to intermolecular antiferromagnetic coupling. The lack of linearity shown in the $1/\chi_M$ data with increasing temperature (Figures S15 and S20) confirms that the data do not follow normal Curie law behavior. Both sets of data show slight curvature that cannot be attributed to temperature independent paramagnetism (TIP). While the curvature could indicate that the complexes are undergoing a prolonged spin state change, where $T_{1/2}$ is higher than the measured temperature range, susceptibility measurements for $[Fe(\mathbf{Tim})](OTf)_3$ at higher temperatures (Figure S16), do not show an upturn in $\chi_M T$ values as the

DOI: 10.1021/acs.inorgchem.8b01022
Inorg. Chem. XXXX, XXX, XXX−XXX

temperature is increased up to 365 K, indicating that any solid-state spin crossover event would require even higher temperatures.

Theoretical Calculations. In order to gain further insight into the magnetic properties, first-principles calculations were carried out for $[Fe(\mathbf{Mim})]^{3+}$ complex.[45] The relative energy of the lowest sextet, quartet, and doublet spin states were first investigated at the scalar relativistic Kohn−Sham (KS) density functional theory (DFT) level with single-point calculations perfomed using the experimental structure. The results are shown in Figure S24, with the corresponding numerical values given in Table S6. The calculations were carried out for different percentages of exact exchange (eX) with the functional B3LYP (the standard parametrization of B3LYP has 20% eX). Without eX, the doublet spin state is calculated to be more stable than the quartet and the sextet by 12 087 and 20 112 cm^{-1}, respectively. The increase of the percentage of eX leads to a strong energetic stabilization of the sextet spin state. With 60% eX, the doublet and sextet spin states are found almost degenerate and the quartet is 5566 cm^{-1} higher. The relative energies of the spin states were also calculated for optimized structures and the results are given in Table S7. For 15% eX, the sextet and the quartet are 1615 and 3709 cm^{-1} above the doublet ground state (GS). However, for 45% eX, the GS corresponds to the sextet spin state, with the doublet and quartet being 7700 cm^{-1} higher. A recommended[46,47] value for the eX fraction in KS calculations of relative spin-state energies is 15%. Therefore, the GS is almost certainly a spin-doublet and excited states with higher spin multiplicity are not thermally accessible.

The electronic structure and the magnetic properties of the Fe(III) complex were also investigated using relativistic all-electron multireference wavefunction theory, including spin−orbit (SO) coupling. The energies of the scalar (SR) and spin−orbit states were calculated at the CASSCF and CASPT2 level for the experimental structure. The main results are shown in Tables 1 and S8−S9. The active space CAS(9,12) corresponds to 9 electrons in the five 3d orbitals, two ligand-centered occupied orbitals that can form bonding and antibonding combinations of local σ symmetry with the "eg" orbitals of the iron center, and a set of 3d′ (pseudo-4d) orbitals to take into account the so-called double-shell effect. The presence of the ligand orbitals and of these 3d′ orbitals in the active space strongly stabilize the excited states compared to a minimal active space of only the 3d orbitals (Table S10). With CASSCF, the GS is a spin-sextet, with the excited doublet and quartet states 1843 and 7592 cm^{-1} above the GS when including SO coupling. The influence of dynamic correlation at the CASPT2 level on the relative energy of the spin states is profound, as already indicated by the KS data (Tables 1 and S6). The PT2 GS corresponds to a spin-doublet, in agreement with the KS calculations for reasonable fractions of eX. At the SR level, the GS corresponds formally to a $^2T_{2g}$ state ($t_{2g}^5e_g^0$ configuration) of the O_h parent symmetry point group, with a triple orbital degeneracy. The deviation from the O_h symmetry in $[Fe(\mathbf{Mim})]^{3+}$ splits this $^2T_{2g}$ state into 3 spin-doublets, with the two excited doublets at 192 and 1037 cm^{-1} above the GS. The M_S components of these SR doublets, along with spin-quartet state components, mix via the SO coupling to give three Kramers doublets, one of them being the SO GS, with the excited doublets calculated at 654 and 1415 cm^{-1} above the GS. The lowest SO states with spin-quartet and -sextet parentage are predicted to be 5160 and 5438 cm^{-1} above the GS, respectively.

The natural orbitals of the SO GS[48,49] of $[Fe(\mathbf{Mim})]^{3+}$ are shown in Figure S25. The occupation numbers for the ground Kramers doublet reflect the formal $t_{2g}^5e_g^0$ configuration corresponding to an idealized octahedral coordination, but with crucial differences. The electron hole, relative to a closed-shell nonmagnetic $t_{2g}^6e_g^0$ configuration, is not evenly distributed over the three t_{2g} 3d orbitals. This is a result of the near, but not exact, degeneracy of these orbitals in the $[Fe(\mathbf{Mim})]^{3+}$ complex. The magnetic properties of the three Kramers doublets that arise from this nearly degenerate set of 3d orbitals are therefore likely to be sensitive to minor perturbations affecting the splitting, which may include static and dynamic solvent effects or molecular vibrations. The small occupations in the formal e_g orbitals are attributed to correlation effects with the corresponding σ bonding orbitals. The calculated electronic g-factors for this SO GS are given in Figure 6 and Table S10. At our best level of calculation, i.e., SO-CAS(9,12)PT2, a large z component of the g tensor is calculated with g_z = 3.845, while g_x and g_y are 0.283 and 1.599. These calculated values are in good agreement with the g-

Table 1. Relative Energy (cm^{-1}) of the Lowest Doublet, Quartet, and Sextet Spin States of $[Fe(Mim)]^{3+}$[a]

	CAS(9,12)SCF		CAS(9,12)PT2	
states	SR	SO	SR	SO
doublet	2160	1843	0	0
quartet	7541	7592	5117	5160
sextet	0	0	5531	5438

[a]CAS(9,12)SCF/PT2 results using X-ray structure.

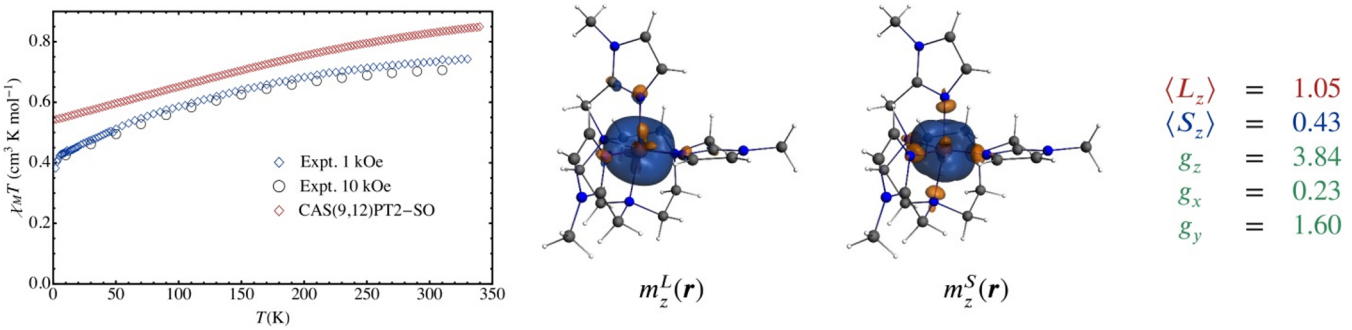

Figure 6. Calculated magnetic susceptibility $\chi_M T$(cm^3 K mol^{-1}) as a function of T (K) for $[Fe(\mathbf{Mim})]^{3+}$. CAS(9,12)PT2-SO Results. Orbital (m_z^L) and spin (m_z^S) magnetization densities and g-factors for the ground-state doublet. Doublet components with $\langle S_z \rangle > 0$. Iso-surfaces values ±0.001 au.

DOI: 10.1021/acs.inorgchem.8b01022
Inorg. Chem. XXXX, XXX, XXX−XXX

factors measured for related Fe(III) complexes that are close to octahedral symmetry.[50] The large magnetic anisotropy arises here from a large unquenched orbital angular momentum ($\langle L_z \rangle$ = 1.05), while the spin angular momentum is close to the expected value of 0.5 for a spin-doublet ($\langle S_z \rangle$ = 0.43). The calculated magnetic susceptibility of $[Fe(\mathbf{Mim})]^{3+}$ is also shown in Figure 6. The quite acceptable agreement with the experimental curves confirm that $[Fe(\mathbf{Mim})]^{3+}$ has a spin-doublet GS and that its effective magnetic moment is higher than predicted for the spin only value because of a large orbital angular momentum component. From the calculated χ_M, one gets a μ_{eff} of 2.58, which is only slightly larger than the experimental value taken from the magnetic susceptibility (μ_{eff} = 2.43).

SUMMARY

The two low-spin Fe(III) complexes reported here produce relatively sharp, paramagnetically shifted resonances. We demonstrate the first examples, to the best of our knowledge, of low-spin mononuclear Fe(III) complexes studied as paraCEST or paraSHIFT agents.[12,13] The macrocyclic nature of the complexes imparts kinetic inertness of the complexes in aqueous solution, even at acidic or alkaline pH values that typically induce dissociation of Fe(III) complexes. $[Fe(\mathbf{Tim})]^{3+}$ complex forms anionic donor groups from the imidazole pendents at high pH that serve to stabilize the Fe(III) center even at pH > 12, whereas $[Fe(\mathbf{Mim})]^{3+}$ complex is stable toward dissociation only at pH from 3 to 8.

The compact coordination environment with six nitrogen donors produced by **Mim** and **Tim** ligands strongly stabilizes Fe(III) versus Fe(II). Redox potentials range from 328 mV vs NHE for the $[Fe(\mathbf{Mim})]^{3+}$ complexes, whereas the Fe(III) complex of **Tim** has redox potentials of 320 to −270 mV vs NHE depending on protonation state. In contrast, TACN ligands with three pendant pyridine derivatives produce complexes that stabilize divalent Fe(II) centers with redox potentials close to 1 V vs NHE, regardless of whether the Fe(II) center is high- or low-spin.[15,51] Thus, the Fe(III) complexes here with appended imidazoles might be paired with their Fe(II) analogs as examples of redox activated paraCEST or paraSHIFT agents.

Both $[Fe(\mathbf{Mim})]^{3+}$ and $[Fe(\mathbf{Tim})]^{3+}$ have low-spin Fe(III) centers as shown by magnetic susceptibility measurements in solution and in the solid state. Magnetic susceptibility measurements in the solid state give μ_{eff} = 2.3 and 2.4, respectively for $[Fe(\mathbf{Tim})]^{3+}$ and $[Fe(\mathbf{Mim})]^{3+}$ at 300 K. In solution, the experimental magnetic moments are μ_{eff} = 2.8 or 3.0 for $[Fe(\mathbf{Tim})]^{3+}$ and $[Fe(\mathbf{Mim})]^{3+}$, respectively, at neutral pH and 298 K in solution. These large magnetic moments are supported by theoretical calculations for the ground state of S = 1/2 parentage. Calculated magnetic susceptibilities confirm that there is a substantial orbital angular momentum present that produces magnetic moments much higher than the spin-only value. The magnetic moments of the complexes in solution are slightly higher than those in the solid state, which may be due to interactions with solvent that affect the geometry of the complexes and magnetic susceptibility compared to that in the solid state. For example, there is only one diastereomeric form of $[Fe(\mathbf{Mim})](OTf)_3$ in the solid state as shown by the crystal structure. The ^{1}H resonances of $[Fe(\mathbf{Mim})]^{3+}$ are consistent with a single diastereomeric form in solution. $[Fe(\mathbf{Tim})]^{3+}$ also has a ^{1}H NMR spectrum at acidic pH which is consistent with a single predominant diastereomeric form. However, we cannot rule out the presence of a small proportion of a second diastereomeric form in solution as is often the case for this type of macrocyclic complex.[3,52,53] Indeed the broadening of the proton resonances of the complexes at higher temperatures suggests that a second diastereromeric form is energetically accessible in solution. Improvements in the rigidity of the complexes will be important for these complexes to be further developed for biomedical applications as paramagnetic probes. For example, strategically placed methyl groups in the pendent arms have been shown to produce rigid complexes for transition metal complexes with the TACN macrocycle framework.[3,37]

As shown here, the $[Fe(\mathbf{Tim})]^{3+}$ complex is not an effective paraCEST agent. The Fe(III) center does not produce a significant paramagnetic shift of the imidazole pendent NH proton, and the CEST peak is only discernible at acidic pH (5.7) at 25 °C and broadens as the temperature is increased to 37 °C. These observations suggest that the exchange rate constant is too large for the modest shift of the CEST peak. Furthermore, the large Lewis acidity of the Fe(III) center increases the acidity of the imidazole NH protons such that one of the imidazole pendants is ionized at neutral pH. This result highlights the challenges associated with using low-spin Fe(III) complexes as paraCEST agents. The donor groups that produce CEST must be chosen with care to take into account the more facile ionization of the exchangeable NH proton in trivalent iron complexes compared to divalent transition metal ion complexes. The more modest paramagnetic induced shifts of the proton resonances of the low-spin Fe(III) center in comparison to high-spin Fe(II) also present a challenge to the development of these complexes as paraCEST agents, as it is important to substantially shift the CEST peak to avoid interference from magnetization transfer effects.[16,54]

EXPERIMENTAL SECTION

Instrumentation. A Varian Inova 500 MHz NMR spectrometer equipped with FTS Systems TC-84 Kinetics Air Jet Temperature Controller was used to collect ^{1}H NMR spectra. ^{13}C NMR spectra were acquired using a Varian Mercury 300 MHz NMR spectrometer operating at 75 MHz. A 4.7 T MRI scanner (ParaVision 3.0.2, Bruker Biospin, Billerica MA) using a 60 cm (I.D.) gradient insert and a 35 mm (I.D.) quadrature radiofrequency coil (m2m imaging, Cleveland, OH) was used for T_1 measurements on $[Fe(\mathbf{Tim})]^{3+}$. Temperature was maintained at 37 °C during imaging using an MR-compatible heating system (SA Instruments, Stony Brook, NY). A Fisher Scientific accumet micro glass mercury-free combination pH electrode connected to a Thermo Scientific Orion Star A211 pH benchtop meter was used for pH measurements. ThermoFinnigan LCQ Advantage IonTrap LC/MS equipped with a Surveyor HPLC system was used to collect mass spectral data. Absorbance spectra were collected using Beckman-Coulter DU 800 UV−vis Spectrophotometer equipped with a Peltier Temperature Controller. The HypSpec software was used to fit pK_a values as described in the Supporting Information. Cyclic voltammograms were obtained by using a Princeton Applied Research VersaSTAT 3 Potentiostat/Galvanostat operated with VersaStudio software. CHI 104 Glassy Carbon Disk (3 mm) Working Electrode, CHI 111 Ag/AgCl Reference Electrode with porous Teflon Tip, and CHI 115 Platinum Wire Counter Electrode from CH Instruments, Inc. (Austin, TX) were used.

Magnetic susceptibility data were collected using a Quantum Design MPMS XL SQUID magnetometer. Finely ground samples were loaded into polyethylene or polypropylene bags and sealed on the benchtop, and then the bags were inserted into drinking straws. Ferromagnetic impurity checks were performed for each sample by sweeping the field (0−10 kOe) at 100 K: linearity in all plots (Figures

DOI: 10.1021/acs.inorgchem.8b01022
Inorg. Chem. XXXX, XXX, XXX−XXX

S13 and S18) indicated lack of significant ferromagnetic impurities. Static (dc) magnetic susceptibility data were collected at temperatures ranging from 2 to 365 and 330 K for $[Fe(\mathbf{Tim})]^{3+}$ and $[Fe(\mathbf{Mim})]^{3+}$, respectively, at applied fields of 1 and 10 kOe. Magnetization measurements were collected at 1.8 K, while varying the applied field up to 50 kOe. Data were corrected for the magnetization of the sample holder by subtracting the susceptibility of an empty container, and for diamagnetic contributions of the sample by using Pascal's constants.[55]

Computational Details. Relativistic *ab initio* wave function calculations were carried out with a developer's prerelease 8 version of Molcas.[45] The second-order Douglas−Kroll−Hess scalar relativistic Hamiltonian[56] was employed in the calculations without spin−orbit (SO) coupling. The all electron ANO-RCC Gaussian-type orbital (GTO) basis sets from the Molcas library were used for the ligand atoms. The ANO-RCC basis sets were contracted to TZP quality for the metal center and for the surrounding nitrogen atoms (Fe = 21s15p10d6f4g2h/6s5p3d2f1g ; N = 14s9p4d3f2g/4s3p2d1f). A DZP contraction was used for the carbon atoms (C = 14s9p4d3f2g/3s2p1d; H = 8s4p3d1f/2s1p). The computations used state-averaged CASSCF (Complete Active Space Self-Consistent Field).[57] SO coupling was treated by state interactions between the CASSCF wave functions, using the Restricted Active Space State Interaction (RASSI) program.[58] The influence of dynamic correlation effects was investigated by using CASPT2 (Complete Active Space Perturbation Theory at second order).[59] The CASPT2 calculations were performed using the multistate approach with a real shift of 0.2 in order to avoid intruder states. A local modification of Molcas was used to generate electron density natural orbitals (NOs), and the spin magnetizations from the SO wave functions.[48,49,60] Iso-surfaces of the orbitals were created and visualized with the graphical user interface of the Amsterdam Density Functional (ADF) suite.[61,62] Additional all-electron scalar relativistic Kohn−Sham (KS) DFT calculations were carried out with ADF, using the zero-order regular approximation (ZORA) Hamiltonian and triple-ζ doubly polarized (TZ2P) Slater-type orbital basis sets along with the B3LYP hybrid functional.[63−66] For these KS calculations, different values of the exact exchange percentage were investigated (B3LYP proper has 20%).[46]

The CAS calculations were performed first using an active space CAS(5,5) which corresponds to the 5 electrons of the Fe^{3+} ion spanning the five 3d orbitals. This active space was then augmented with two doubly occupied ligand orbitals to form CAS(9,7). Finally, CAS(9,7) was then augmented with the addition of five 3d′ orbitals to form CAS(9,12) in order to take into account the double-shell effect.[67] The orbitals included in the active space are shown in Figure S25. Such a computational strategy has been successfully applied recently to describe the magnetic anisotropy of Iron(III) complexes.[50] The state-average calculations were performed for several scalar spin-states, i.e., one sextet, six quartets, and 12 doublets.

Crystallization and X-ray Diffraction Data Collection. The crystals of $[Fe(\mathbf{Mim})](OTf)_3$ were obtained by slow evaporation of acetonitrile solution at −4 °C. A clear intense purple-orange plate-like specimen of $C_{24}H_{33}F_9FeN_9O_9S_3$, approximate dimensions 0.16 × 0.54 × 0.60 mm, was used for the X-ray crystallographic analysis. Single-crystal X-ray data of were collected on a Bruker VENTURE Photon-100 CMOS diffractometer at 173 K with APEX 2 software suite; absorption correction was applied using SADABS,[68] the structures were solved by the direct methods using SHELXT[69] and was refined using the SHELXL-2014[70] program package. In crystal structures reported in this work, all non-hydrogen atoms were refined anisotropically; hydrogen atoms were refined with riding coordinates with U_{iso} = 1.5 U_{iso}(C) for methyl groups and U_{iso} = 1.2 U_{iso}(C) for methylene groups. Structure was refined as an inversion twin with absolute structure parameter of 0.100(12). One of triflate ions shows significant disorder which was modeled using enhanced rigid-bond restraints (RIGU) for the disordered fragment. OLEX2 GUI[71] was employed for all calculations and molecular graphics.

■ ASSOCIATED CONTENT

Supporting Information

The Supporting Information is available free of charge on the ACS Publications website at DOI: 10.1021/acs.inorgchem.8b01022.

Experimental details including NMR spectra, UV−vis spectra, CEST spectra, crystallographic tables, and experimental and synthetic procedures are available (PDF)

Accession Codes

CCDC 1835939 contains the supplementary crystallographic data for this paper. These data can be obtained free of charge via www.ccdc.cam.ac.uk/data_request/cif, or by emailing data_request@ccdc.cam.ac.uk, or by contacting The Cambridge Crystallographic Data Centre, 12 Union Road, Cambridge CB2 1EZ, UK; fax: +44 1223 336033.

■ AUTHOR INFORMATION

Corresponding Author

*E-mail: jmorrow@buffalo.edu. Fax 716-645-6963.

ORCID

Pavel B. Tsitovich: 0000-0002-3916-936X
Alexander Y. Nazarenko: 0000-0003-0916-0636
Matthew P. Shores: 0000-0002-9751-0490
Jochen Autschbach: 0000-0001-9392-877X
Janet R. Morrow: 0000-0003-4160-7688

Notes

The authors declare no competing financial interest.

■ ACKNOWLEDGMENTS

J.R.M. thanks the NSF (CHE-1310374 and CHE-1710224) for support of this work. B.N.L. and M.P.S. thank the NSF (CHE-1363274) for support. J.A. acknowledges NSF grant CHE-1560881 for financial support for the theoretical part of this article. We thank Dr. Joseph Spernyak of Roswell Park Cancer Institute for T_1 measurements.

■ REFERENCES

(1) Dorazio, S. J.; Tsitovich, P. B.; Siters, K. E.; Spernyak, J. A.; Morrow, J. R. Iron(II) PARACEST MRI Contrast Agents. *J. Am. Chem. Soc.* **2011**, *133*, 14154−14156.

(2) Tsitovich, P. B.; Cox, J. M.; Spernyak, J. A.; Morrow, J. R. Gear Up for a pH Shift: A Responsive Iron(II) 2-Amino-6-picolyl-Appended Macrocyclic paraCEST Agent That Protonates at a Pendent Group. *Inorg. Chem.* **2016**, *55*, 12001−12010.

(3) Tsitovich, P. B.; Cox, J. M.; Benedict, J. B.; Morrow, J. R. Six-coordinate Iron(II) and Cobalt(II) paraSHIFT Agents for Measuring Temperature by Magnetic Resonance Spectroscopy. *Inorg. Chem.* **2016**, *55*, 700−716.

(4) Dorazio, S. J.; Morrow, J. R. Iron(II) complexes containing octadentate tetraazamacrocycles as paraCEST magnetic resonance imaging contrast agents. *Inorg. Chem.* **2012**, *51*, 7448−7450.

(5) Dorazio, S. J.; Olatunde, A. O.; Tsitovich, P. B.; Morrow, J. R. Comparison of divalent transition metal ion paraCEST MRI contrast agents. *JBIC, J. Biol. Inorg. Chem.* **2014**, *19*, 191−205.

(6) Olatunde, A. O.; Bond, C. J.; Dorazio, S. J.; Cox, J. M.; Benedict, J. B.; Daddario, M. D.; Spernyak, J. A.; Morrow, J. R. Six, Seven or Eight Coordinate Fe(II), Co(II) or Ni(II) Complexes of Amide-Appended Tetraazamacrocycles for ParaCEST Thermometry. *Chem. - Eur. J.* **2015**, *21*, 18290−18300.

(7) Du, K.; Waters, E. A.; Harris, T. D. Ratiometric quantitation of redox status with a molecular Fe_2 magnetic resonance probe. *Chem. Sci.* **2017**, *8*, 4424−4430.

DOI: 10.1021/acs.inorgchem.8b01022
Inorg. Chem. XXXX, XXX, XXX−XXX

(8) Jeon, I.-R.; Park, J. G.; Haney, C. R.; Harris, T. D. Spin crossover iron(II) complexes as PARACEST MRI thermometers. *Chem. Sci.* **2014**, *5*, 2461−2465.
(9) Thorarinsdottir, A. E.; Gaudette, A. I.; Harris, T. D. Spin-crossover and high-spin iron(II) complexes as chemical shift ^{19}F magnetic resonance thermometers. *Chem. Sci.* **2017**, *8*, 2448−2456.
(10) Schwert, D. D.; Richardson, N.; Ji, G.; Raduchel, B.; Ebert, W.; Heffner, P. E.; Keck, R.; Davies, J. A. Synthesis of two 3,5-disubstituted sulfonamide catechol ligands and evaluation of their iron(III) complexes for use as MRI contrast agents. *J. Med. Chem.* **2005**, *48*, 7482−7485.
(11) Kuznik, N.; Wyskocka, M. Iron(III) Contrast Agent Candidates for MRI: a Survey of the Structure-Effect Relationship in the Last 15 Years of Studies. *Eur. J. Inorg. Chem.* **2016**, *2016*, 445−458.
(12) Tsitovich, P. B.; Morrow, J. R. Macrocyclic ligands for Fe(II) paraCEST and chemical shift MRI contrast agents. *Inorg. Chim. Acta* **2012**, *393*, 3−11.
(13) Morrow, J. R.; Tsitovich, P. B. Transition Metal paraCEST Probes as Alternatives to Lanthanides. In *Chemical Exchange Saturation Transfer Imaging: Advances and Applications*; Pan Stanford Publishing: 2017; pp 257−282.
(14) Tsitovich, P. B.; Tittiris, T. Y.; Cox, J. M.; Benedict, J. B.; Morrow, J. R. Fe(II) and Co(II) N-methylated CYCLEN complexes as paraSHIFT agents with large temperature dependent shifts. *Dalton Trans.* **2018**, *47*, 916−924.
(15) Dorazio, S. J.; Tsitovich, P. B.; Gardina, S. A.; Morrow, J. R. The reactivity of macrocyclic Fe(II) paraCEST MRI contrast agents towards biologically relevant anions, cations, oxygen or peroxide. *J. Inorg. Biochem.* **2012**, *117*, 212−219.
(16) Olatunde, A. O.; Cox, J. M.; Daddario, M. D.; Spernyak, J. A.; Benedict, J. B.; Morrow, J. R. Seven-coordinate Co(II), Fe(II) and six-coordinate Ni(II) amide-appended macrocyclic complexes as ParaCEST agents in biological media. *Inorg. Chem.* **2014**, *53*, 8311−8321.
(17) de Martino Norante, G.; Di Vaira, M.; Mani, F.; Mazzi, S.; Stoppioni, P. Transition metal complexes of a functionalised triazamacrocycle. *J. Chem. Soc., Dalton Trans.* **1992**, 361−365.
(18) Di Vaira, M.; Mani, F.; Stoppioni, P. Co-ordination of 1,4,7-tris(pyrazol-3-ylmethyl)-1,4,7-triazacyclononane with iron(III), nickel(II) and zinc(II). Crystal and molecular structures of $[ML][ClO_4]_2\ nH_2O$ (M = Ni, n= 0.5; M = Zn, n= 1). *J. Chem. Soc., Dalton Trans.* **1994**, 3739−3743.
(19) Auerbach, U.; Eckert, U.; Wieghardt, K.; Nuber, B.; Weiss, J. Synthesis and Coordination Chemistry of the Hexadentate Ligands 1,4,7-Tris(2-Hydroxybenzyl)-1,4,7-Triazacyclononane (H_3L^1) and 1,4,7-Tris(3-Tert-Butyl-2-Hydroxybenzyl)-1,4,7-Triazacyclononane (H_3L^2). Crystal Structures of $[HL^1Cu^{II}]$ and $[L^2Fe^{III}]$acacH. *Inorg. Chem.* **1990**, *29*, 938−944.
(20) Auerbach, U.; Weyhermuller, T.; Wieghardt, K.; Nuber, B.; Bill, E.; Butzlaff, C.; Trautwein, A. X. First-row transition metal complexes of the hexadentate macrocycle 1,4,7-tris(5-*tert*-butyl-2-hydroxybenzyl)-1,4,7-triazacyclononane (LH_3). Crystal structures of $[LTi^{IV}]BPh_4$, $[LCr^{III}]$, $[LFe^{III}]$, and $[(LH)_2Fe^{III}{}_2](ClO_4)_2.2H_2O$. *Inorg. Chem.* **1993**, *32*, 508−519.
(21) Snodin, M. D.; Ould-Moussa, L.; Wallmann, U.; Lecomte, S.; Bachler, V.; Bill, E.; Hummel, H.; Weyhermüller, T.; Hildebrandt, P.; Wieghardt, K. The Molecular and Electronic Structure of Octahedral Tris(phenolato)iron(III) Complexes and Their Phenoxyl Radical Analogues: A Mössbauer and Resonance Raman Spectroscopic Study. *Chem. - Eur. J.* **1999**, *5*, 2554−2565.
(22) Stockheim, C.; Hoster, L.; Weyhermuller, T.; Wieghardt, K.; Nuber, B. First-row transition-metal complexes of mixed 'pendant-arm' derivatives of 1,4,7-triazacyclononane containing phenolate and carboxylate functional groups. *J. Chem. Soc., Dalton Trans.* **1996**, 4409−4416.
(23) Luckay, R.; Hancock, R. D.; Cukrowski, I.; Reibenspies, J. H. Study of protonation of 1,4,7-tris(2-hydroxyethyl)-1,4,7-triazacyclononane, and its complexes with metal ions, by crystallography, polarography, potentiometry, molecular mechanics and NMR. *Inorg. Chim. Acta* **1996**, *246*, 159−169.
(24) Bernhardt, P. V.; Chen, K. I.; Sharpe, P. C. Transition metal complexes as mediator-titrants in protein redox potentiometry. *J. Biol. Inorg. Chem.* **2006**, *11*, 930−936.
(25) Hatfield, T. L.; Staples, R. J.; Pierce, D. T. Structure Change Associated with the $[M^{II/III}$ 1,4,7-Triazacyclononane-N,N′,N″-triacetate (TCTA)$]^{-/0}$ Electron Transfers (M = Mn, Fe, and Ni): Crystal Structure for $[Fe^{II}(H_2O)_6][Fe^{II}(TCTA)]_2$. *Inorg. Chem.* **2010**, *49*, 9312−9320.
(26) Schlager, O.; Wieghardt, K.; Nuber, B. Trivalent Transition Metal Complexes $[M^{III}(L\text{-}3H)]$ (M = Fe, Co) of the Triply Deprotonated Hexadentate Ligand 1,4,7-Tris(*o*-aminobenzyl)-1,4,7-triazacyclononane (L). Crystal Structure of $[Mn^{IV}(L\text{-}3H)]BPh_4$. *Inorg. Chem.* **1995**, *34*, 6456−6462.
(27) Boeyens, J. C. A.; Forbes, A. G. S.; Hancock, R. D.; Wieghardt, K. Crystallographic Study of the Low-Spin Iron(II) and Iron(III) Bis Complexes of 1,4,7-Triazacyclononane. *Inorg. Chem.* **1985**, *24*, 2926−2931.
(28) Sabenya, G.; Lazaro, L.; Gamba, I.; Martin-Diaconescu, V.; Andris, E.; Weyhermuller, T.; Neese, F.; Roithova, J.; Bill, E.; Lloret-Fillol, J.; Costas, M. Generation, Spectroscopic, and Chemical Characterization of an Octahedral Iron(V)-Nitrido Species with a Neutral Ligand Platform. *J. Am. Chem. Soc.* **2017**, *139*, 9168−9177.
(29) Tsitovich, P. B.; Kosswattaarachchi, A. M.; Crawley, M. R.; Tittiris, T. Y.; Cook, T. R.; Morrow, J. R. An Fe^{III} Azamacrocyclic Complex as a pH-Tunable Catholyte and Anolyte for Redox-Flow Battery Applications. *Chem. - Eur. J.* **2017**, *23*, 15327−15331.
(30) Lambert, F.; Policar, C.; Durot, S.; Cesario, M.; Yuwei, L.; Korri-Youssoufi, H.; Keita, B.; Nadjo, L. Imidazole and Imidazolate Iron Complexes: On the Way for Tuning 3D-Structural Characteristics and Reactivity. Redox Interconversions Controlled by Protonation State. *Inorg. Chem.* **2004**, *43*, 4178−4188.
(31) Sunatsuki, Y.; Ohta, H.; Kojima, M.; Ikuta, Y.; Goto, Y.; Matsumoto, N.; Iijima, S.; Akashi, H.; Kaizaki, S.; Dahan, F.; Tuchagues, J.-P. Supramolecular Spin-Crossover Iron Complexes Based on Imidazole−Imidazolate Hydrogen Bonds. *Inorg. Chem.* **2004**, *43*, 4154−4171.
(32) Burns, P. J.; Cox, J. M.; Morrow, J. R. Imidazole-Appended Macrocyclic Complexes of Fe(II), Co(II), and Ni(II) as ParaCEST Agents. *Inorg. Chem.* **2017**, *56*, 4545−4554.
(33) Gotzmann, C.; Braun, F.; Bartholoma, M. D. Synthesis, ^{64}Cu-labeling and PET imaging of 1,4,7-triazacyclononane derived chelators with pendant azaheterocyclic arms. *RSC Adv.* **2016**, *6*, 119−131.
(34) Baker, J.; Engelhardt, L. M.; Figgis, B. N.; White, A. H. Crystal structure, electron spin resonance, and magnetism of tris(*o*-phenanthroline)iron(III) perchlorate hydrate. *J. Chem. Soc., Dalton Trans.* **1975**, 530−534.
(35) Di Vaira, M.; Mani, F.; Stoppioni, P. A new general route to the synthesis of polyazamacrocyclic ligands with pendant biomimetic imidazole groups. *J. Chem. Soc., Chem. Commun.* **1989**, 126−127.
(36) Zang, Y.; Kim, J.; Dong, Y. H.; Wilkinson, E. C.; Appelman, E. H.; Que, L. Models for Nonheme Iron Intermediates: Structural Basis for Tuning the Spin States of Fe(TPA) Complexes. *J. Am. Chem. Soc.* **1997**, *119*, 4197−4205.
(37) Abozeid, S. M.; Snyder, E. M.; Tittiris, T. Y.; Steuerwald, C. M.; Nazarenko, A. Y.; Morrow, J. R. Inner-Sphere and Outer-Sphere Water Interactions in Co(II) paraCEST Agents. *Inorg. Chem.* **2018**, *57*, 2085−2095.
(38) Harvey, P.; Blamire, A. M.; Wilson, J. I.; Finney, K.-L. N. A.; Funk, A. M.; Senanayake, P. K.; Parker, D. Moving the goal posts: enhancing the sensitivity of PARASHIFT proton magnetic resonance imaging and spectroscopy. *Chem. Sci.* **2013**, *4*, 4251−4258.
(39) Tsitovich, P. B.; Spernyak, J. A.; Morrow, J. R. A Redox-Activated MRI Contrast Agent that Switches Between Paramagnetic and Diamagnetic States. *Angew. Chem., Int. Ed.* **2013**, *52*, 13997−14000.

DOI: 10.1021/acs.inorgchem.8b01022
Inorg. Chem. XXXX, XXX, XXX−XXX

(40) Evans, D. F. 400. The determination of the paramagnetic susceptibility of substances in solution by nuclear magnetic resonance. *J. Chem. Soc.* **1959**, 2003−2005.
(41) Yatsunyk, L. A.; Walker, F. A. Structural, NMR, and EPR Studies of S = 1/2 and S = 3/2 Fe(III) Bis(4-Cyanopyridine) Complexes of Dodecasubstituted Porphyrins. *Inorg. Chem.* **2004**, *43*, 757−777.
(42) Ortega-Villar, N.; Guerrero-Estrada, A. Y.; Piñeiro-López, L.; Muñoz, M. C.; Flores-Álamo, M.; Moreno-Esparza, R.; Real, J. A.; Ugalde-Saldivar, V. M. Spin Crossover Behavior in a Series of Iron(III) Alkoxide Complexes. *Inorg. Chem.* **2015**, *54*, 3413−3421.
(43) Vieira, B. J. C.; Coutinho, J. T.; Santos, I. C.; Pereira, L. C. J.; Waerenborgh, J. C.; da Gama, V. [Fe($nsal_2$trien)]SCN, a New Two-Step Iron(III) Spin Crossover Compound, with Symmetry Breaking Spin-State Transition and an Intermediate Ordered State. *Inorg. Chem.* **2013**, *52*, 3845−3850.
(44) Nihei, M.; Shiga, T.; Maeda, Y.; Oshio, H. Spin crossover iron(III) complexes. *Coord. Chem. Rev.* **2007**, *251*, 2606−2621.
(45) Aquilante, F.; Autschbach, J.; Carlson, R. K.; Chibotaru, L. F.; Delcey, M. G.; De Vico, L.; Fdez. Galván, I.; Ferré, N.; Frutos, L. M.; Gagliardi, L.; et al. Molcas 8: New capabilities for multiconfigurational quantum chemical calculations across the periodic table. *J. Comput. Chem.* **2016**, *37*, 506−541.
(46) Reiher, M.; Salomon, O.; Hess, B. A. Reparameterization of hybrid functionals based on energy differences of states of different multiplicity. *Theor. Chem. Acc.* **2001**, *107*, 48−55.
(47) Harvey, J. N. DFT Computation of Relative Spin-State Energetics of Transition Metal Compounds. In *Principles and Applications of Density Functional Theory in Inorganic Chemistry I*; Kaltsoyanis, N., McGrady, J. E., Eds.; Springer-Verlag: Berlin Heidelberg, 2004; pp 151−184.
(48) Gendron, F.; Páez-Hernández, D.; Notter, F.-P.; Pritchard, B.; Bolvin, H.; Autschbach, J. Magnetic Properties and Electronic Structure of Neptunyl(VI) Complexes: Wavefunctions, Orbitals, and Crystal-Field Models. *Chem. - Eur. J.* **2014**, *20*, 7994−8011.
(49) Autschbach, J. Orbitals for Analyzing Bonding and Magnetism of Heavy-Metal Complexes. *Comments Inorg. Chem.* **2016**, *36*, 215−244.
(50) Ridier, K.; Mondal, A.; Boilleau, C.; Cador, O.; Gillon, B.; Chaboussant, G.; Le Guennic, B.; Costuas, K.; Lescouëzec, R. Polarized Neutron Diffraction to Probe Local Magnetic Anisotropy of a Low-Spin Fe(III) Complex. *Angew. Chem., Int. Ed.* **2016**, *55*, 3963−3967.
(51) Wieghardt, K.; Schoffmann, E.; Nuber, B.; Weiss, J. Syntheses, properties and electrochemistry of transition-metal complexes of the macrocycle 1,4,7-tris(2-pyridylmethyl)-1,4,7-triazacyclononane (L). Crystal structures of [NiL]$(ClO_4)_2$, [MnL]$(ClO_4)_2$, and [PdL]$(PF_6)_2$ containing a distorted-square-base-pyramidal $Pd^{II}N_5$ core. *Inorg. Chem.* **1986**, *25*, 4877−4883.
(52) Huskens, J.; Sherry, A. D. Co-ordination chemistry and molecular mechanics study of the magnesium(II) and calcium(II) complexes of trisubstituted 1,4,7-triazacyclononane derivatives. *J. Chem. Soc., Dalton Trans.* **1998**, *0*, 177−184.
(53) Neil, E. R.; Funk, A. M.; Yufit, D. S.; Parker, D. Synthesis, stereocontrol and structural studies of highly luminescent chiral tris-amidepyridyl-triazacyclononane lanthanide complexes. *Dalton Trans.* **2014**, *43*, 5490−5504.
(54) Li, A. X.; Hudson, R. H. E.; Barrett, J. W.; Jones, C. K.; Pasternak, S. H.; Bartha, R. Four-pool modeling of proton exchange processes in biological systems in the presence of MRI−paramagnetic chemical exchange saturation transfer (PARACEST) agents. *Magn. Reson. Med.* **2008**, *60*, 1197−1206.
(55) Bain, G. A.; Berry, J. F. Diamagnetic corrections and Pascal's constants. *J. Chem. Educ.* **2008**, *85*, 532−536.
(56) Wolf, A.; Reiher, M.; Hess, B. A. The generalized Douglas−Kroll transformation. *J. Chem. Phys.* **2002**, *117*, 9215−9226.
(57) Roos, B. O.; Taylor, P. R.; Siegbahn, P. E. M. A complete active space SCF method (CASSCF) using a density matrix formulated super-CI approach. *Chem. Phys.* **1980**, *48*, 157−173.
(58) Malmqvist, P. Å.; Roos, B. O.; Schimmelpfennig, B. The restricted active space (RAS) state interaction approach with spin−orbit coupling. *Chem. Phys. Lett.* **2002**, *357*, 230−240.
(59) Andersson, K.; Malmqvist, P. A.; Roos, B. O.; Sadlej, A. J.; Wolinski, K. Second-order perturbation theory with a CASSCF reference function. *J. Phys. Chem.* **1990**, *94*, 5483−5488.
(60) Gendron, F.; Pritchard, B.; Bolvin, H.; Autschbach, J. Single-ion 4f element magnetism: an *ab-initio* look at $Ln(COT)_2^-$. *Dalton Trans.* **2015**, *44*, 19886−19900.
(61) te Velde, G.; Bickelhaupt, F. M.; Baerends, E. J.; Fonseca Guerra, C.; van Gisbergen, S. J. A.; Snijders, J. G.; Ziegler, T. Chemistry with ADF. *J. Comput. Chem.* **2001**, *22*, 931−967.
(62) Fonseca Guerra, C.; Snijders, J. G.; te Velde, G.; Baerends, E. J. Towards an order-N DFT method. *Theor. Chem. Acc.* **1998**, *99*, 391−403.
(63) Becke, A. D. Density-Functional Thermochemistry. III. The Role of Exact Exchange. *J. Chem. Phys.* **1993**, *98*, 5648−5652.
(64) Lee, C. T.; Yang, W. T.; Parr, R. G. Development of the Colle-Salvetti Correlation-Energy Formula into a Functional of the Electron-Density. *Phys. Rev. B: Condens. Matter Mater. Phys.* **1988**, *37*, 785−789.
(65) Vosko, S. H.; Wilk, L.; Nusair, M. Accurate spin-dependent electron liquid correlation energies for local spin density calculations: A critical analysis. *Can. J. Phys.* **1980**, *58*, 1200−1211.
(66) Stephens, P. J.; Devlin, F. J.; Chabalowski, C. F.; Frisch, M. J. *Ab Initio* Calculation of Vibrational Absorption and Circular Dichroism Spectra Using Density Functional Force Fields. *J. Phys. Chem.* **1994**, *98*, 11623−11627.
(67) Kepenekian, M.; Robert, V.; Le Guennic, B.; De Graaf, C. Energetics of $[Fe(NCH)_6]^{2+}$ via CASPT2 calculations: A spin-crossover perspective. *J. Comput. Chem.* **2009**, *30*, 2327−2333.
(68) Krause, L.; Herbst-Irmer, R.; Sheldrick, G. M.; Stalke, D. Comparison of silver and molybdenum microfocus X-ray sources for single-crystal structure determination. *J. Appl. Crystallogr.* **2015**, *48*, 3−10.
(69) Sheldrick, G. M. SHELXT - Integrated space-group and crystal-structure determination. *Acta Crystallogr., Sect. A: Found. Adv.* **2015**, *71*, 3−8.
(70) Sheldrick, G. M. Crystal structure refinement with SHELXL. *Acta Crystallogr., Sect. C: Struct. Chem.* **2015**, *71*, 3−8.
(71) Dolomanov, O. V.; Bourhis, L. J.; Gildea, R. J.; Howard, J. A. K.; Puschmann, H. OLEX2: a complete structure solution, refinement and analysis program. *J. Appl. Crystallogr.* **2009**, *42*, 339−341.

DOI: 10.1021/acs.inorgchem.8b01022
Inorg. Chem. XXXX, XXX, XXX−XXX